Quantitative Evaluation of an Automated Cone-based Breast Ultrasound Scanner for MRI – 3D US Image Fusion

Anton V. Nikolaev, Leon de Jong, Gert Weijers, Vincent Groenhuis, Ritse M. Mann, Françoise J. Siepel, Bogdan M. Maris, Stefano Stramigioli, *Fellow, IEEE*, Hendrik H.G. Hansen, *Member, IEEE*, Chris L. de Korte, *Senior Member, IEEE*

***Abstract*— Breast cancer is one of the most diagnosed types of cancer worldwide. Volumetric ultrasound breast imaging, combined with MRI can improve lesion detection rate, reduce examination time, and improve lesion diagnosis. However, to our knowledge, there are no 3D US breast imaging systems available that facilitate 3D US – MRI image fusion. In this paper, a novel Automated Cone-based Breast Ultrasound System (ACBUS) is introduced. The system facilitates volumetric ultrasound acquisition of the breast in a prone position without deforming it by the US transducer. Quality of ACBUS images for reconstructions at different voxel sizes (0.25 and 0.50 mm isotropic) was compared to quality of the Automated Breast Volumetric Scanner (ABVS) (Siemens Ultrasound, Issaquah, WA, USA) in terms of signal-to-noise ratio (SNR), contrast-to-noise ratio (CNR), and resolution using a custom made phantom. The ACBUS image data were registered to MRI image data utilizing surface matching and the registration accuracy was quantified using an internal marker. The technology was also evaluated in vivo. The phantom-based quantitative analysis demonstrated that ACBUS can deliver volumetric breast images with an image quality similar to the images delivered by a currently commercially available Siemens ABVS. We demonstrate on the phantom and in vivo that ACBUS enables adequate MRI-3D US fusion. To our conclusion, ACBUS might be a suitable candidate for a second-look breast US exam, patient follow-up, and US guided biopsy planning.**

This study has received funding by the European Union's Horizon 2020 research and innovation program under grant agreement no. 688188 as part of the MURAB project.

Anton V. Nikolaev, Leon de Jong, Gert Weijers, Ritse M. Mann, Hendrik H. G. Hansen, and Chris L. de Korte are with Medical Ultrasound Imaging Center (MUSIC), Department of Medical Imaging, Radboud University Medical Center, Nijmegen, 6525 GA the Netherlands (e-mail: anton.nikolaev@radboudumc.nl, Leon.deJong@radboudumc.nl, Gert.Weijers@radboudumc.nl, Ritse.Mann@radboudumc.nl, Rik.Hansen@radboudumc.nl, Chris.deKorte@radboudumc.nl).

Vincent Groenhuis, Françoise J. Siepel, Stefano Stramigioli, and Chris L. de Korte are with University of Twente, Enschede, 7522 NB the Netherlands (e-mail: groenhuis@gmail.com, f.j.siepel@utwente.nl, s.stramigioli@utwente.nl).

Bogdan M. Maris is with Department of Computer Science, Università degli Studi di Verona, Verona, 37129 Italy (e-mail: bogdan.maris@univr.it).

Index Terms—Breast, Phantom, Image Fusion, Image Quality, 3D US

I. INTRODUCTION

BREAST cancer is one of the most diagnosed type of cancer and the second cause of cancer death in the female population [1]. Furthermore, one has to realize that 4% of invasive breast cancers is diagnosed in women under 40 years old [2]. Several studies show that breast cancer in young women is more aggressive than in women over 40 years old [3, 4]. Many of these cancers occur in women at increased risk, who are annually screened. However, mammography has poor performance in this group since breast tissue is much denser than in older women. Consequently, other techniques, particularly contrast enhanced breast MRI, are recommended for adequate diagnosis of women at a high risk [5].

Breast examination includes most of the time an ultrasound (US) examination. It is a popular low-cost imaging modality for breast cancer detection due to its high usability and sensitivity. US is the most cost-effective tool for biopsy guidance and therapeutic monitoring [6]. US is often used as a complementary screening tool [7, 8], as well as a second-look [9] imaging modality for otherwise detected abnormalities. The second-look 2D US examination has a high clinical value as an add-on to MRI. Several studies demonstrated that the sensitivity and specificity for tumor detection are improved by enabling the correlation between the lesions' appearances in US and MRI [10-13]. It drives the decision on further patient management leading either to biopsy or follow-up avoiding over-diagnosis and, consequently, overtreatment. [11, 14]. However, 2D US imaging is limited by the field of view, operator-dependency, and low reproducibility that complicates patient follow-up. Furthermore, examination is required to be performed by a radiologist familiar with MRI to image the corresponding region [10, 11].

Volumetric US imaging does not have the abovementioned shortcomings. It is increasingly being used in breast imaging [15-18]. Compared to 2D Breast US, 3D Breast US depends less on the operator and also reduces examination time. It gives a better anatomic overview of the breast interior and facilitates quantitative volumetric lesion analysis [17, 19]. Furthermore, it substantially simplifies follow-up of patients with lesions,

clearly visible in US [11]. Therefore, a volumetric ultrasound breast imaging system that also enables MRI – 3D US image fusion will provide better breast diagnosis by reducing operator-dependency, improving robustness of the second-look US examination and follow-up.

There are several ultrasound systems available that facilitate breast volumetric imaging. A 3D Breast US acquisition utilizing the ACUSON S2000 Automated Breast Volume Scanner (ABVS) [18] (Siemens Ultrasound, Issaquah, WA, USA) is performed by translating a 2D ultrasound transducer over a breast while a woman is in the supine position. The 2D images are stacked to form a volume afterwards [16]. A similar approach is used in the Invenia Automated Breast Ultrasound System (ABUS) that employs a concave ultrasound transducer array (Invenia ABUS, GE Healthcare, Sunnyvale, CA, USA)[18]. Shipley et al. described a system for volumetric imaging of the breast with women in prone-position using a conical container with a conventional linear 38 mm transducer array [20]. The cone's angle was 45° and the breast was deformed by the container during the scanning procedure. The Sofia system (Hitachi Medical Systems GmbH, Wiesbaden, Germany) uses an US transducer array also at a slight angle revolving around the prone breast, positioned in the semi-spherical cap, deforming the breast [15]. The benefit of the Sofia system as well as the system described by Shipley is that women are scanned in prone position, which implies that the geometry of the breast more closely resembles that of the breast during MRI scanning than with the two systems that scan in the supine position. All abovementioned systems, however, perform breast scanning while the breast is in a highly deformed state, making the fusion between MRI and 3D US data challenging and requiring the use of sophisticated registration and fusion techniques. Such so-called deformable models have already been implemented to register MRI to X-ray mammograms [21], which are typically acquired while compressing the breast between two plates. Another study [22] describes a registration method facilitating prone to supine breast registration. However, in both cases the boundary conditions such as the pressure between plates or the gravitational force are known. Unfortunately, the boundary conditions for current volumetric ultrasound devices are unknown, which makes the application of deformable models challenging. To our knowledge there are no studies published that report a successful registration between prone MRI and volumetric ultrasound breast images acquired with one of the aforementioned devices.

An alternative ultrasound-based breast imaging modality is ultrasound computed tomography (USCT) [23]. USCT facilitates visualization of the speed of sound, ultrasound transmission coefficient, and attenuation of the breast tissue resulting in high sensitivity to detect lesions, comparable to MRI [24]. Several fully operational clinical and research prototypes that enable USCT have already been developed: USCT II described by Ruiter at al. in [25], a ring 3D ultrasound system from Chang Liu et al. [26], and a quantitative breast tissue tomography device from Wiskin et al. [27]. Furthermore, there are at least two commercially available USCT systems: the SoftVue system (Delphinus Medical Technologies, Inc, Novi, MI, USA)[28], and the QT Ultrasound system (QT Ultrasound LLC, Novato, CA, USA)[29]. For all abovementioned USCT systems, the patient is in prone position on the examination bed with the breast inside a cup filled with water as a coupling medium. To our knowledge, there is no study about USCT published that demonstrates successful MRI – 3D US image fusion. Besides, USCT is currently still a non-real time modality which impedes its usage in applications for therapeutic control or surgical navigation.

In this paper, we describe and evaluate a novel Automated Cone-based Breast Ultrasound System (ACBUS) that acquires volumetric ultrasound data of the breast in a prone position with only minor deformation, thus facilitating MRI – 3D US fusion. The great benefit of this approach is that the breast position is similar to the MRI acquisition [30]. The performance of the ACBUS in terms of image quality was evaluated quantitatively utilizing a custom-developed phantom and compared with the image quality obtained with a conventional S2000 ABVS. Finally, the technology was evaluated in vivo on a volunteer with a diagnosed cyst and a fibroadenoma.

II. MATERIALS AND METHODS

A. Phantom Design

For quantification of the image quality in volumetric images, we used a custom-made quantitative breast phantom (QBP). The structure of the QBP is depicted in Fig. 1. It includes 8 lesions of different echogenicity with each a diameter of 15 mm and a wire with a diameter of 0.35 mm. The lesions and the wire are embedded in background material.

All lesions and the background material were fabricated by dissolving polyvinyl alcohol (PVA, Acros organics, Geel, Belgium) (10% by weight) in a cooling liquid (CL) - solution of ethylene glycol (40% by volume) (Ethylene glycol, Sigma-Aldrich, Zwijndrecht, the Netherlands) and distilled water (60% by volume) - at 90 °C, while stirring with a magnetically steered stirring rod at 500 rpm for 1.5 hours. For acoustic scattering, the Silica gel 60 particles (Merck KGaA, Darmstadt, Germany) were added to the solution 10 min before starting the cooling process while stopping stirring. The resulting PVA solution was used for further manufacturing steps.

The lesions were fabricated in advance. To achieve different echogenicity levels per lesion, both the concentration and the size of the silica particles were varied. The use of different particle sizes was needed since the concentration higher than 5% did not establish the desirable increase in echo intensity level. The particle concentration and the sizes used for the manufacturing of the lesions are listed in Table I. The lesions' PVA solution was poured in spherical molds, cooled until room

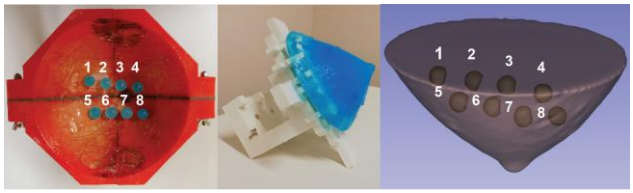

(a) (b) (c)

Fig. 1. Design of the QBP. (a) The lesions fixed inside the breast mold. (b) The manufactured QBP. (c) A rendered MRI image of the QBP.

TABLE I
COMPOSITION OF THE LESIONS IN THE QBP

Lesion #	PVA (%)	CL (%)	SP (%)	SP size (μm)	Lesion Intensity (dB)
1	10	89	1	63 – 100	8.2
2	10	89	1	40 – 63	7.1
3	10	85	5	<40	3.1
4	10	88	2	<40	-1.3
5	10	88.5	1.5	<40	-3.3
6	10	89	1	<40	-4.4
7	10	89.5	0.5	<40	-5.1
8	10	90	0	NA	-22.8
BG	6.5	91.5	2	<40	0

PVA = polyvinyl alcohol, CL = cooling liquid, SP = silica particles, NA = not applicable, BG = background

temperature and went through one freeze-thaw cycle. The lesions were positioned in the breast solution using strings attached to the walls of the breast mold (Fig. 1a).

Next, the PVA solution prepared as a background material was poured in the breast mold at 50°C. After the PVA solution reached room temperature, the mold was stored in a freezer at -24°C for 16 hours to undergo a freeze cycle and subsequently thawed. So, the lesions underwent 2 freeze-thaw cycles and the surrounding material only 1. The wire was inserted into the phantom after the manufacturing had been finalized.

The nominal lesion intensity of the QBP with respect to the background was determined by referencing the intensity of the QBP to that of a commercially available ATS M550 phantom (ATS Labs Inc., Bridgeport, CT, USA) with lesions of known echo intensities. Five images per lesion and background were acquired in both phantoms with a Siemens P500 US system (Siemens Ultrasound, Issaquah, WA, USA) as shown in Fig. 2. The images were exported in DICOM format. The data were analyzed with QA4US software [31] after applying a beam-profile correction (BPC) and lookup table (LUT) correction [32]. The following relation was used to estimate the nominal intensity of the lesions, I_l^{QBP}:

$$I_l^{QBP} = \frac{g_l^{QBP} - g_b^{QBP}}{\gamma^{ref}}. \quad (1)$$

Herein the gamma factor γ^{ref} was estimated based on the ATS M550 phantom measurements using the protocol described in [33]; g_l^{QBP} is the average gray level value of a lesion in the QBP; g_b^{QBP} is the average gray level value of the background in the QBP.

B. In Vivo Measurements

To demonstrate the feasibility of the ACBUS in the clinical routine in vivo measurements were performed. A female volunteer (30 years old) was selected for the study, who was previously diagnosed with a cyst located close to the nipple and a fibroadenoma, located in the lower outer quadrant of the breast.

C. Measurement Protocol

First, the QBP and the volunteer were scanned with a Siemens Skyra 3-Tesla MRI system (Siemens Healthcare, Erlangen, Germany) utilizing a conventional MRI protocol for breast screening. Specifically, the images acquired with a T1 sequence and a Dixon protocol (fat series) [34] were used for in vivo measurements. During the MRI scanning of the volunteer, the breast was immersed in a water container fit in a breast coil. Utilizing water is not a part of the routine breast magnetic resonance imaging protocol. However, this step was needed to assist the registration and avoid the need for deformation modeling. Next, the QBP and the volunteer were scanned using custom-developed ACBUS and conventional ABVS.

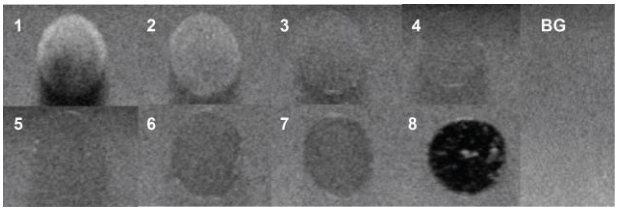

Fig. 2. US images of the lesions inside the QBP acquired with the Siemens P500 US system. BG denotes background.

The measurement protocol was approved by the local ethics committee and in accordance with the World Medical Association Declaration of Helsinki on Ethical Principles for Medical Research Involving Human Subjects. The volunteer agreed to participate and a written informed consent was obtained.

D. System Design

The developed ACBUS is based on the abovementioned Siemens ACUSON S2000 ABVS. The 14L5BV transducer array (Siemens Medical Solutions, Mountain View, CA, USA) of 152 mm length was detached from the Breast ABVS robotic arm (Siemens Medical Solutions, Mountain View, CA, USA) and integrated in the wall of a 3D printed polylactide (PLA, Ultimaker B.V., Geldermalsen, the Netherlands) cone-shaped container ("cone") with no PLA material blocking the surface of the transducer array (Fig. 3d).The "cone" has an opening with a diameter of 160 mm and an angle of 90°, to accommodate breasts of cup size A and B to be positioned inside the "cone" without any contact either with the wall of the container or the transducer's surface (Fig. 3c). The side of the "cone" has a length of ~113 mm, thus, part of the transducer is enclosed by the PLA of the conical container. The part of the probe Δx is

Fig. 3. ACBUS design overview: a – the examination table with a hole for breast positioning; b – Siemens S2000 ABVS system; c – the 14L5BV transducer; d – the cone-shaped PLA container; e – the waterproof umbrella for motor protection; f – the stepper motor; g – the ABVS robotic arm; h – the stepper motor control unit; i – dimensions of the "cone".

not used for imaging because the ultrasound signal is blocked by the PLA material (Fig. 3i). The "cone" can accommodate a breast in the prone position and is located underneath the examination table. During the US acquisition, the "cone" was filled with physiological saline solution (0.9% salt, 99.1% distilled water) as a coupling medium between the breast and the transducer. The "cone" was actuated by a closed loop stepper motor ARM69AC (Oriental Motor, Torrance, USA) (Fig. 3f). In this prototype system, a PVA umbrella (Fig. 3e) was included to protect the motor from water ingress. Spatial calibration was not required since the geometry of the "cone" was known [35]. The design of the "cone" ensures its axis matches the axis of the motor.

The system was classified as an electrically safe device and approved by the local ethical committee for use in patients.

The operation of ACBUS did not differ from that of the ABVS. The scanning can be initiated by pressing the button in the ABVS arm (Fig. 3g) and the US B-mode image acquisition is synchronized with the motion of the container. Therefore, no additional temporal calibration was required [35]. The acquired and anonymized DICOM data were transferred for further processing from the ultrasound machine to an off-line workstation using a memory stick.

The ACBUS system enables the Cartesian and Radial views of the acquired 3D US data. The Cartesian view is applied to the reconstructed data while the Radial view assumes viewing of the originally acquired US images. Besides, ACBUS facilitates the real-time US imaging with the Radial view.

E. Ultrasound Data Acquisition

As aforementioned, the US data of the QBP and the volunteer were obtained with both the novel ACBUS (Fig. 4a) and the standard ABVS (Fig. 4b) .

With respect to ACBUS, the "cone" performed a full rotation around the QBP or the breast, while continuously acquiring ultrasound B-mode data for multiple 2D planes. The rotation speed was 0.07 rad/s. During the acquisitions, both, the QBP and the breast were not touched by the transducer.

In case of the conventional ABVS acquisition, the transducer is linearly translated over a distance of 167 mm with a constant velocity of 1.9 mm/s while acquiring ultrasound B-mode data for multiple parallel 2D planes. The transducer is placed in the plastic case as shown in Fig. 4b. A replaceable acoustically transparent membrane is attached to the bottom of the case (Fig. 4b). The membrane prevents the breast from protruding into the plastic case, where it would impede the translation of the transducer. During the scanning, optimal contact between the transducer and the QBP or the breast was achieved by deforming it with the membrane.

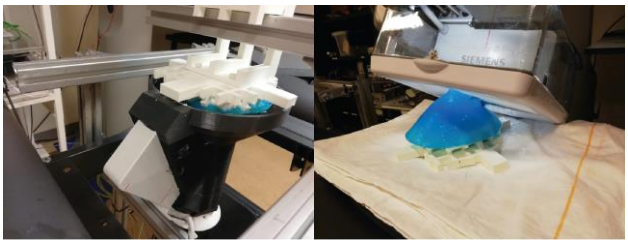

(a) (b)

Fig. 4. Scanning of the QBP. (a) ACBUS. (b) ABVS. In case of the ABVS acquisition the US transducer moves inside a box with an interfacing membrane.

Imaging settings in the ACUSON S2000 system for the acquisitions with both, ACBUS and ABVS, were equal and are reported in Table II. TGC sliders were set to the middle position. In total, 309 images were acquired at a frame rate of ~3.5 Hz over a duration of 90 s. The exceptionally low framerate is a result of the huge number of elements (4 to 5 times higher than regular handheld transducers), due to compounding of image data using 3 beam-steered transmits, and due to using multiple transmit foci. Each image consisted of 537 x 682 pixels with a pixel size of 0.1 mm axially x 0.2 mm laterally. One ACBUS scan sufficed to capture all lesions of the QBP. For ABVS, two acquisitions were required to scan all lesions. The transducer has a central frequency of 9 MHz and two focal points (at 1.5 cm and at 4.5 cm) were used during transmission.

F. Volumetric Reconstruction

ABVS volumetric data were reconstructed by stacking acquired B-mode images together in the elevation direction. The reconstructed volume ranged between -76 and 76 mm along the x-axis (lateral), 0 and 162 mm along the y-axis (elevational), and 0 and 60 mm along the z-axis (axial) with a voxel size of 0.2mm x 0.5mm x 0.1mm (the standard resolution of the embedded ABVS reconstruction).

To reconstruct the ACBUS volume, first, the coordinates of each pixel of the acquired images were transformed from the local US transducers coordinate system into the world coordinate system by an affine transformation as depicted in Fig. 5:

$$H_i = R_y\left(\frac{\alpha}{2}\right) \cdot R_z(i \cdot \theta) \cdot \begin{bmatrix} 1 & 0 & 0 & 0.5 \cdot l_{tr} - \Delta x \\ 0 & 1 & 0 & 0 \\ 0 & 0 & 1 & 0 \\ 0 & 0 & 0 & 1 \end{bmatrix}, \quad (2)$$

where θ is the angular spacing between two consequently acquired B-mode images ($\theta \approx 1.16^{o}$), i is the number of the acquired images, Δx is the length of the excess area beyond the conical container ($\Delta x \approx 113$ mm), R_y and R_z are the 4x4 transformation matrixes representing rotations around the y and z axis, respectively, and l_{tr} is the length of the US transducer array ($l_{tr} \approx 152$ mm).

Next, the coordinates of all transformed pixels were combined to form a point cloud:

$$p = \bigcup_{i=1}^{N} H_i \cdot p_i^0, \quad (3)$$

where p_i^0 represents the coordinates of all pixels within the B-mode image, N is the number of acquired images, and p is the resulting point cloud.

TABLE II
SETTINGS IN THE ACUSON SIEMENS S2000

Preset	MaxDepth (mm)	Freq (MHz)	TCE	Map
D+	60	9	Off	F

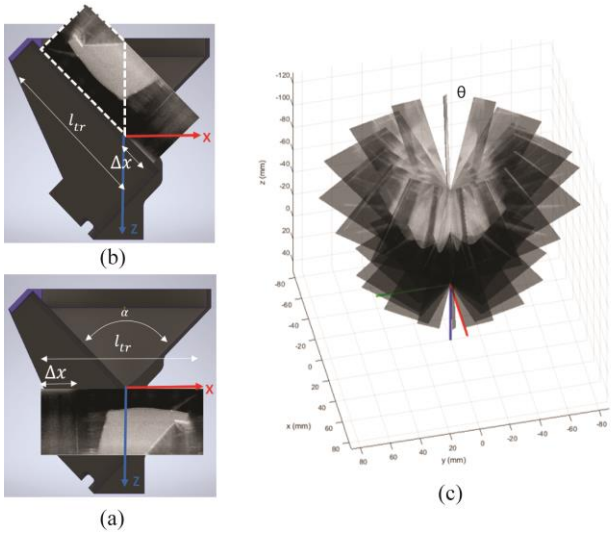

Fig. 5. Affine transformations steps of the ultrasound frame in the "cone's" coordinate system for the volumetric reconstruction. (a) Initial position. (b) Single frame rotated around the y – axis. (c) Frames rotated around the z – axis. The dashed line denotes the region of interest for the 3D reconstruction.

Only pixels within the region of interest (ROI) shown by the dashed line in Fig. 5 were included in the point cloud. The ROI was selected such that only image data corresponding to the area in between the transducer and the rotation axis of the cone were used for the reconstruction. Next, each voxel of a pre-defined voxel grid was assigned with a mean intensity value of the pixels within the point cloud that belong to the voxel's volume. Since some voxels can remain unassigned, a "hole filling" step was used [36]. It has been shown before [37] that linear interpolation methods perform best in terms of trade-off between reconstruction speed and delivered image quality. Hence, a linear interpolation was selected for the "hole filling".

The reconstruction was implemented with Matlab2019 (MatWorks, Natick, USA) on a PC equipped with an Intel Xeon CPU (2x2.40GHz) and 64 GB RAM. The reconstruction was done for several isotropic voxel sizes (IVS): 0.25 mm (minimum voxel size limited by available RAM), 0.50 mm to investigate how the image quality was affected and to show how much time was spent on each reconstruction step. The volume for the reconstruction was ranged from -86 to 86 mm along the x-axis (lateral), from -86 to 86 mm along the y-axis (elevational), and from -129 to 0 mm along the z-axis (axial). The percentage of holes and time performance was determined for each case and each reconstruction step.

The angular spacing between the imaging planes leads to undersampling of the volume close to the edge of the cone. With the current angular spacing θ of 1.16° the distance between two neighboring planes is 1.62 mm at a radius of 80 mm from the cone's axis and 0.81 mm at 40 mm.

G. Image Registration

ACBUS (IVS of 0.25 mm) and MRI volumetric images were fused together utilizing surface matching based on iterative closest point algorithm (ICP) [38]. As a measure of the registration accuracy, we calculated the Dice coefficient and the distance between the geometrical centers of the cysts (-22.8 dB lesion in QBP) in the MRI and 3D US data after the image fusion for the phantom and in vivo data. The cysts in MRI and 3D US data were segmented semi-automatically utilizing a region growing algorithm. The volumes of the segmented lesions was calculated. Besides, we calculated the Root Mean Squared Error (RMSE) between the matched point clouds representing breast surfaces segmented in MRI and 3D US images. All abovementioned metrics were calculated with Matlab2019 while the segmentation was done with 3D Slicer v4.10.2 [39].

H. Contrast and Noise

Performance of both ACBUS (IVS of 0.25 mm) and ABVS was compared quantitatively by calculating contrast-to-noise ratio (CNR) and signal-to-noise ratio (SNR) [40] defined as:

$$CNR = 20log_{10}\frac{|\mu_l - \mu_b|}{\sqrt{0.5(\sigma_l{}^2+\sigma_b{}^2)}} \quad (4)$$

and

$$SNR = 20log_{10}\frac{\mu_l}{\sigma_l}, \quad (5)$$

where μ_l and μ_b are the mean echo levels within the lesion and background areas, respectively, σ_l and σ_b are the standard deviations of the echo levels within the lesion and the background, respectively. The paired differences in SNR and CNR values between ACBUS (reference, reconstructed data at 0.25 mm and 0.50 mm IVS) and ABVS data were calculated, denoted as ΔSNR and ΔCNR, respectively. A Kruskal-Wallis test (N = 8) was applied to determine if there was a statistically significant difference in ΔSNR and ΔCNR between the various reconstruction settings.

All acquired images delivered by both, ACBUS and ABVS, were pre-processed before the reconstruction for objective performance of gray level quantitative analysis. First, depth dependent attenuation correction was applied to each image. Regarding the data acquired with ACBUS scanner, the coupling medium gap between the transducer and the phantom was corrected for [41]. Next, each image was normalized to the average background gray level value within the QBP. The result of the pre-processing step is shown in Fig. 6. Each lesion was segmented manually by fitting spheres inside the lesions with 3D Slicer v4.10.2. The background reference region was also determined manually by segmenting a sphere of equal diameter next to each lesion. The combined background gray levels for all the reference lesions was used for the CNR calculation.

Due to the manufacturing process, some lesions contained void areas resulting in artefacts within the area of the segmented lesion. For objective quantitative evaluation, the segmented gray level signal within each lesion from both ACBUS and ABVS acquisitions was filtered frame-wise by excluding the pixels belonging to the background and outlier signal (bubble or foreign reflector). The pixels within the sliding window were classified as background signal if condition 6 was satisfied:

$$|\mu_w - \mu_b| < \sigma_b, \quad (6)$$

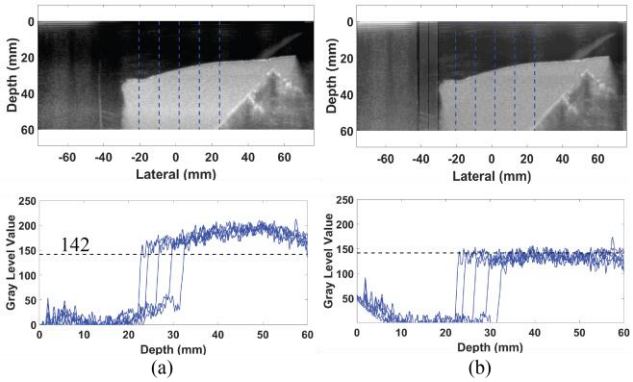

Fig. 6. Cross sections of the QBP acquired with ACBUS. (a) Before pre-processing. (b) After pre-processing. The blue dashed lines on the top images represent locations from which the beam profiles were taken. The dashed black line depicts a reference gray level value of 142.

where μ_w denotes the mean gray level value within the window (6 x 6 pixels), μ_b and σ_b are the mean value and the standard deviation of the background area. The pixels were classified as outliers if their mean gray level value differed from the mean value within the lesion's area (excluding the earlier detected background) by more than $2\sigma_b$.

Quantitative analysis was performed for the upper half of the segmented lesion to exclude the highly attenuated zone. The lesion's half was determined by taking the upper half of the lesion's closest to the transducer surface in both the ACBUS and ABVS volumes.

To understand how the reconstruction with different voxels size affects the image quality, the CNR and SNR within the lesion as well as the standard deviation level of the background were calculated for ACBUS and compared to the CNR and SNR determined based on the ABVS datasets.

I. Resolution

The resolution is an important characteristic of any imaging system and it is of great importance to understand the effect of the reconstruction on the image resolution. For ACBUS the resolution was defined as the size of the line spread function (LSF) measured in the axial and lateral directions as described in [32]. To measure the LSF we selected 3 imaging planes: the middle plane was transversal to the wire and 2 plains had an angular distance of $\pm\,\theta$ from the middle pane. The measurement was repeated 5 times resulting in 15 images with a clearly visible reflector. The LSF was measured in a reference imaging planes before reconstruction, representing an ABVS acquisition. Next, the LSF was measured in a cross-sectional images taken from the same planes of the volume reconstructed with IVS of 0.25 mm and 0.50 mm. A Wilcoxon test (N = 15) was applied to determine a statistical significance of the paired difference in resolution between the ACBUS data before (reference) and after 3D reconstruction.

III. Results

A. Volumetric reconstruction

A rendered volumetric ultrasound image of the QBP is shown in Fig. 7. Table III presents the reconstruction metrics including time consumed per each reconstruction step.

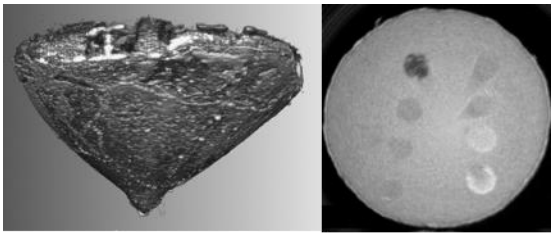

Fig. 7. (a) Reconstructed volumetric image of the QBP at 0.25 mm IVS, and (b) coronal cross section of the volume.

TABLE III
RECONSTRUCTION METRICS FOR ACBUS

ACBUS isotropic voxel size (mm)	Averaging step time (s)	'Hole Filling' step time (s)	Percentage of "holes" (%)
0.25	27	1167	65
0.50	11	198	34

B. Quantitative Comparison

Echo images of the inclusions for both ACBUS at the IVS of 0.25 mm and ABVS are shown in Fig. 8. The SNR and CNR as a function of the lesion echo intensity for ACBUS and ABVS acquisitions are presented in Fig. 9. Table IV shows the dependency of image quality parameters on the voxels size. Both ΔSNR and ΔCNR seemed to increase with increased voxel size, although the Kruskal-Wallis test only showed a statistically significant difference for the reconstruction at IVS of 0.50 mm compared to the ACBUS data before reconstruction, i.e. $\Delta SNR_{0.50}$ ($\Delta SNR_{0.50} = SNR_{ACBUS\ (0.50\ mm\ IVS)} - SNR_{ABVS}$) compared to $\Delta SNR_{\ reference}$. The fact that the other differences were not statistically significant might be related to the relatively small sample size (N = 8).

The influence of the volumetric reconstruction on the resolution is presented in Fig. 10. No statistically significant difference was detected in both the axial and lateral resolution between ABVS and ACBUS for the 0.25 mm IVS. However, the lateral resolution of the ACBUS data reconstructed with the 0.50 mm IVS was significantly worse. The influence of the

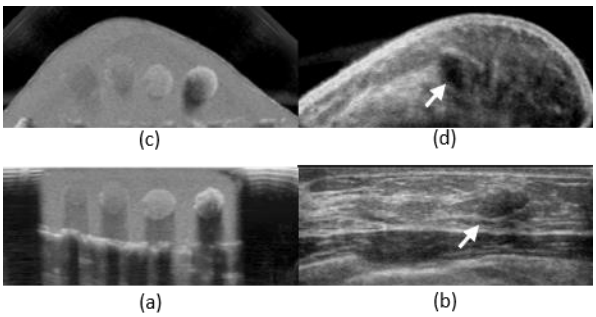

Fig. 8. Cross-sectional images of the QBP and in vivo breast acquired with ACBUS (0.25 mm IVS) and ABVS. (a) QBP scanned with ABVS. (b) In vivo breast scanned with ABVS. (c) QBP scanned with ACBUS. (d) In vivo breast scanned with ACBUS. The white arrow indicates the cyst within in vivo data.

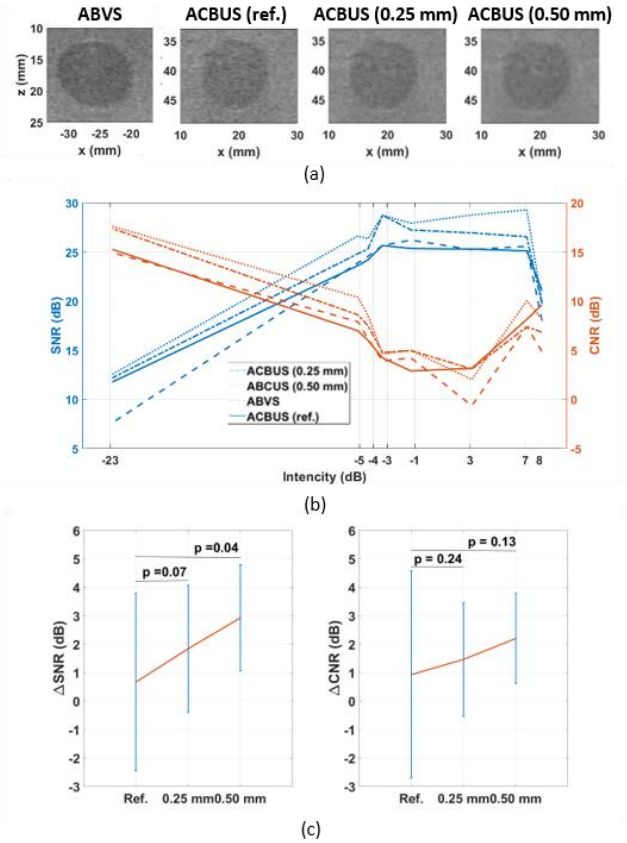

Fig. 9. Influence of the image voxel size on the image quality. (a) Appearance of the -4.4 dB lesion on the ABVS image, on the originally acquired image with ACBUS, and on the reconstructed images for different voxel sizes. (b) SNR and CNR dependency on the lesions echogenicity for ABVS data, ACBUS data before reconstruction ACBUS (ref.), and reconstructed ACBUS data with 0.25 and 0.50 mm IVS. (c) The mean value of paired difference in SNR (ΔSNR) and CNR (ΔCNR) values between ABVS and ACBUS (reference, and reconstructed data with 0.25 mm and 0.50 mm IVS). The red line represents the mean difference while blue indicates the 95% confidence interval.

TABLE IV
DEPENDENCY OF IMAGE QUALITY ON THE VOXEL SIZED USED FOR THE RECONSTRUCTION

US Volume Type	σ_b (gray level)	ΔCNR (dB)	ΔSNR (dB)
ABVS	7.8	0	0
ACBUS			
reference	8.3	0.9±2.2	0.7±1.9
0.25	6.9	1.5±1.2	1.8±1.3
0.50	5.7	2.2±1.0	2.9±1.1

σ_b = standard deviation of the background signal, ΔCNR and ΔSNR = paired difference in CNR, SNR between ABVS and ACBUS (reference, 0.25 mm IVS, and 0.5 mm IVS) data

reconstruction on the image quality in vivo is presented in Fig. 11 .

C. Image Registration

The calculated registration metrics are presented in the Table V. The visualized overlapped cysts are shown in Fig. 12. The overlap between the cists in both, volunteer and the phantom data, is evident.

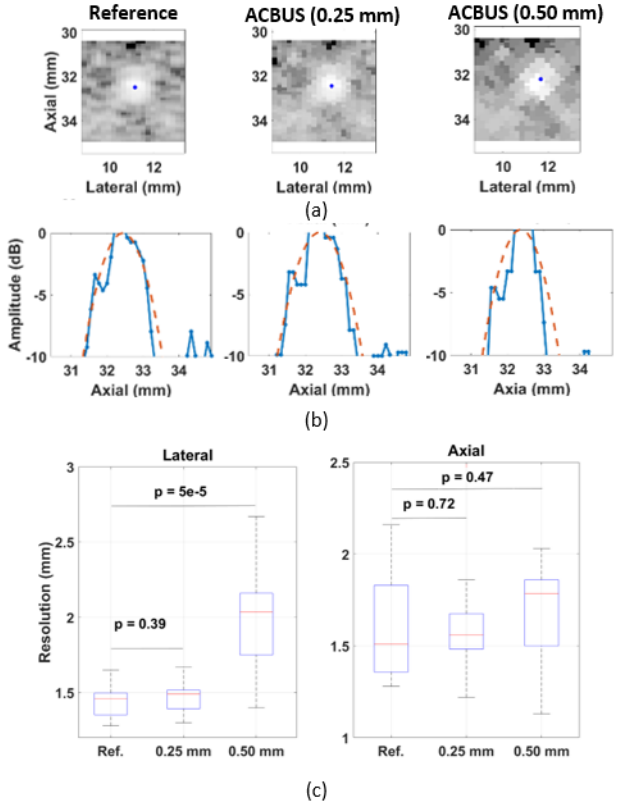

Fig. 10. Effect of the voxel size used for reconstruction on the resolution of the system. (a) Visualized LSF taken from the same imaging plane before and after reconstruction for IVS of 0.25 mm and 0.50 mm. The blue dot indicates the geometrical center of the reflector. (b) LSF in the axial direction for all cases. (c) Boxplot of the estimated resolutions in the lateral and axial directions for all cases.

D. In vivo measurements

The in vivo data are presented in Fig. 13 and Fig. 14. For the MRI and ACBUS images, the same cross-sections were taken for clear observation of the fibroadenoma with the Cartesian and Radial views (Fig. 13). Gray areas in the ACBUS ultrasound images represent fat, while bright areas represent glandular tissue. Both fibroadenoma and axilla are visible pointed out with arrows. In the MRI images (T1 sequence Dixon protocol, fat), glandular tissue is represented as a shaded area while bright represents fat. The lesion is characterized by a dark spots. The skin layer is occult in utilized MRI image. The Fig.14 demonstrates a capability of the ACBUS to imaging axilla.

IV. DISCUSSION

In this paper, we present a 3D Automated Cone-based ultrasound approach. The phantom measurement demonstrates that the ACBUS approach provides images with an image quality close to that of the conventional ABVS. Furthermore, from Fig. 8, it can be noticed that for the ACBUS approach, where the transducer moves around the breast, shadows behind the lesions are reduced due to the combination of image data from multiple insonification angles.

The shadow reduction is a useful feature of the imaging system since it can increase the field-of-view behind the

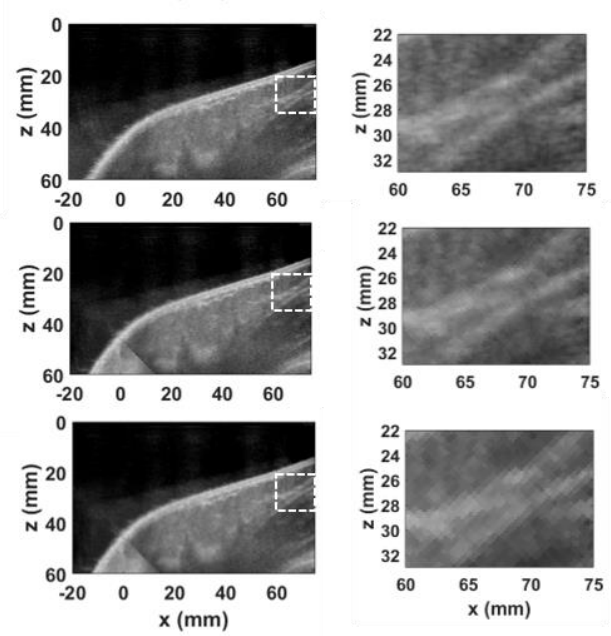

Fig. 11. Influence of the reconstruction on the image quality in the in-vivo data. (top) Image before reconstruction. (middle) Reconstructed with 0.25 mm IVS. (bottom) Reconstructed with 0.50 mm IVS.

shadowing inclusion. However, the acoustic shadow is not completely eliminated still allowing lesion detection and classification [42, 43]. For instance, acoustic shadowing is mostly associated with malignancy. Substantial parts of the shadow at the edges and below the center of lesions still can be imaged with ACBUS, although the true clinical impact of the shadow reduction would need to be investigated in a clinical reader study.

The calculated CNR and SNR values are on average higher for ACBUS compared to ABVS and they keep improving with increasing voxel size. The decrease of the noise level (SNR) and improved contrast (CNR) is a logical consequence of averaging. However, there is no statistically significant difference in the CNR and SNR measured between ABVS and ACBUS for different voxel sizes.

The consequence of the improved SNR and CNR due to the averaging is a loss of resolution. The Wilcoxon tests showed that image resolution was not significantly affected in case of a small voxel size (0.25 mm isotropic). Besides, speckle is visible and its appearance seems (almost) not affected by the reconstruction (Fig. 9, Fig. 10, Fig. 11). However, increasing the voxel size significantly worsens the resolution and fading of the speckle pattern. Therefore, we recommend to use the voxel size with dimensions comparable to the pixel dimensions of the original image.

The standard deviation of the gray levels of the background decreases while the voxel size increases for the ACBUS image data (Table IV). Although the resolution is decreased with the ACBUS approach, the information provided better resembles the information as provided by the MRI as can be clearly seen in Fig. 13 and Fig. 14. The pros and cons of this scanning approach have to be studied in the future. Additionally, the optimal voxel size in terms of resolution and calculation speed needs to be addressed in future studies.

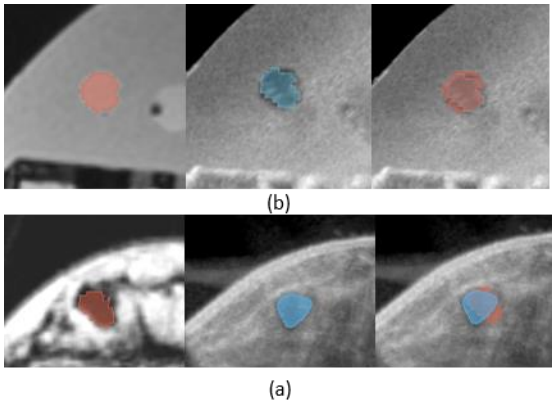

Fig. 12. Result of the MRI – 3D US image registration evaluated with cyst as an internal marker in (a) volunteer and (b) the QBP. From left to right: segmented cyst in MRI, segmented cyst in 3D US, and fused segmentations visualized in 3D US.

TABLE V
REGISTRATION ACCURACY BETWEEN MRI AND 3D US DATA FOR THE QBP AND THE VOLUNTEER

	DSC	d (mm)	RMSE (mm)	$V_{3D\ US}$ (mm^3)	V_{MRI} (mm^3)
QBP	0.70	1.61	0.45	522	805
Volunteer	0.54	2.23	1.04	405	600

DSC = Dice - Sørensen Coefficient, d = distance between the geometrical centers of the segmented cysts, RMSE = Root Mean Squared Error between the matched point clouds representing the breast surfaces segmented in MRI and 3D US, $V_{3D\ US}$ – calculated volume of the cysts' within 3D US data, V_{MRI} – calculated cysts' volume in MRI data.

The undersampling error due to angular spacing did not result in visible deterioration of image quality since the main structure was close to the center of the cone. However, this problem has to be addressed in further implementations. The straightforward solution for this is to decrease the angular stepsize, and, thus, to increase the number of imaging planes. For instance, a 2 times increase of the image acquisition speed can already reduce the linear sampling distance to 0.81 mm at the edge of the "cone".

The registration accuracy metrics, presented in Table V, show the feasibility of MRI – 3D US image fusion with the ACBUS system. The low RMSE and relatively small distance between the centers of the cysts shows the successful registration between MRI and 3D US data. The Dice coefficient is more than 0.50 for both phantom and in vivo data. Therefore, the system can be used to register US-occult lesions in 3D US data for lesion diagnosis. This is an important feature because simultaneous viewing of the same lesion in both modalities can drive the further decision on either follow up, or biopsy. Furthermore, it facilitates follow up of US occult lesions and can prevent over-diagnosis reducing a number of unnecessary MRI-guided biopsies. The Dice coefficient was calculated from the semi-automatic segmented cysts. It can be seen from Table V that the segmentation in MRI has a larger volume. The origin of this mismatch is probably caused by a difference in performance of the region growing algorithm between both modalities. The contrast between the lesion and the background is lower and the resolution is higher on US compared to MRI which results in the relatively smaller lesion segmentation on US. However, from Fig. 12, the overlap between the cysts is evident. Furthermore, the correspondence between the MRI and ACBUS images of the volunteer is evident (Fig. 13). The

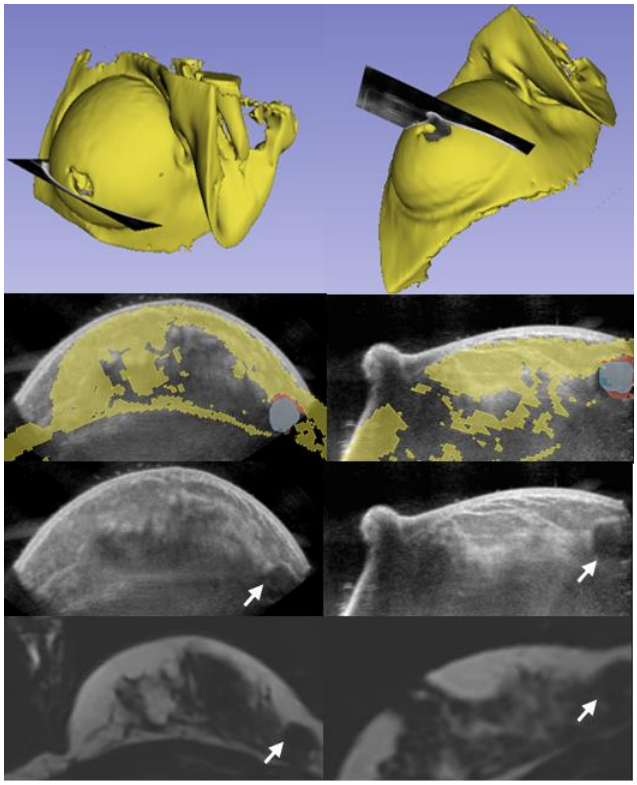

Fig. 13. Simultaneous display of MRI and ACBUS data in (a) Cartesian view and (b) Radial view. From bottom to top: MRI cross-sectional data, ACBUS cross-sectional data, the cross-sectional image of MRI data superimposed on the ACBUS data (fibroadenoma segmented in MRI is indicated with red while the fibroadenoma segmented in US is indicated with blue) , and finally the rendered MRI data with an US plane. The white arrows point at the fibroadenoma.

fibroadenoma was localized in the MRI and ACBUS in the lower part of the breast. The US cross-sectional planes with MRI overlay in both, Cartesian and Radial views, matches very well with fat layer in US data. The slight difference in breast shape is caused by the upward pressure induced by the water in the container and due to the pressure induced by the edges of the slightly different container utilized for MRI scanning. However, it did not seem to deteriorate the registration substantially.

The scan time with ACBUS will remain the same regardless of breast cup size and only limited by the US acquisition framerate and the angular velocity of the motor as will be explained next.

The current version of the ACBUS is not yet applicable to breast with cup sizes larger than B due to the fact that the clinical scanning presets on the S2000 system limit the penetration depth of the US transducer to ~60 mm. This also was the reason why we did not put effort in reducing the size of the transducer fixation that in the current setup blocks ~35% of the imaging view. The data for this part of the imaging view are simply discarded in the current configuration. However, by increasing the penetration depth, and reducing the size of the transducer fixation, it is possible to use the full 152 mm width of the transducer, and scan breast with cup sizes up to D without additional scan time. The penetration depth can be increased by using ultrafast ultrasound scanning as demonstrated by

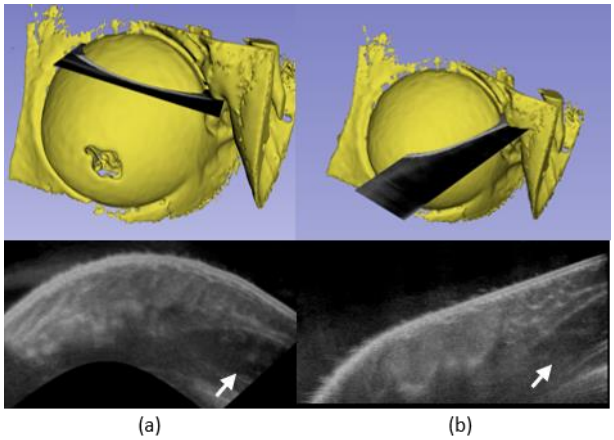

Fig. 14. Imaging of axilla (indicated with a white arrow) with ACBUS in (a) Cartesian view and (b) Radial view.

Holländer et al. [44]. Coherent compounding of ultrafast transmits acquired at 21 angles increased penetration depth without loss of image quality. Furthermore, our group recently showed for a handheld 14L5 transducer, which has the same specs as the 14L5BV transducer, that coherent compounding of ultrafast transmit at 11 angles improves the penetration depth by 20 mm without decreasing resolution.

However, ACBUS can image a major structure of breast, including the axilla that can be seen from the Fig. 14. Aforementioned modifications will also improve imaging of the axilla since a wider area of the chest can be imaged. Besides, a large portion of the retromammary area can already be imaged with the current version of the ACBUS as demonstrated in Fig. 13a. However, the field of view is limited to the area around the central axis of the container and also the image depth is currently limited (Fig. 14a). This area can be extended by incorporating the abovementioned coherent compounding of ultrafast transmits which will increase the penetration depth such that the tissue beyond the cones base can be imaged. By also steering the ultrasound at a small tilt angle it should be possible to enlarge the field-of-view such that all of the relevant retromammary tissue can be imaged.

The difference between ACBUS and ABVS scanners is that in ABVS there is direct contact while in ACBUS there is a variable distance between the transducer surface and the breast. Since the attenuation of the ultrasound signal is much lower in the physiologic saline solution than in real tissue, the automatic time gain compensation of the ultrasound system results in too much amplified echosignals for the breast tissue: the increase in amplitude increases with distance between transducer and breast and thus has to be corrected for. The consequence of this effect can be noticed in Fig. 11 as a variation of brightness around the central line of the cone. An initial correction method was proposed in this study and proved to be effective in homogeneous phantom medium.

As a recommendation for future work, several points can be highlighted to improve the performance of ACBUS. First, it would be useful to implement an adaptive transmission sequence that automatically locates the focal zones next to the skin surface to ensure the ultrasound beam enters the breast without scattered diffraction. Second, as a future improvement, we recommend to use more viscous coupling medium that can reduce reflection at the interface between coupling medium and

skin surface, and give stability to less firm breasts. However, this aspect requires investigation since a medium of too high viscosity might also result in unacceptable force on the breast induced by the rotating cone.

In this study the MRI acquisition was performed while the breast was immersed in a water bath. This was an intermediate solution to facilitate MRI-3D US registration without the need of a non-rigid registration. To enable registration of 3D ACBUS data to standard clinical MRI data acquired without water bath a non-rigid registration method will have to be developed. Non-rigid registration for breast applications have already been successfully employed [21, 22]. Non-rigid registration for ACBUS should be feasible since the boundary conditions, i.e. pressures resulting from the coupling medium, are known.

The substantial difference between ACBUS and its closest commercial analog, the Sofia system, is that the breast is not flattened due to the design of the cone-shaped container accommodating the breast. This critical feature facilitates the fusion of volumetric breast ultrasound with other imaging modalities (e. g. MRI), that is not currently available.

The ACBUS extends the breast scanning approach described by Shipley et al. in [20]. Similar to Shipley's system, with ACBUS the breast is scanned with a conical container. In their system the breast is deformed by the container's wall making the fusion with other modalities challenging. This is not the case for ACBUS which does not deform the breast and makes registration and fusion to other modalities straightforward.

The ACBUS system also facilitates a Radial view of the breast. Thus, it can be also used for therapy monitoring and for a real time US guided biopsy. Besides, the volumetric reconstruction time is short and can be further improved by increased computer power and algorithm optimization. Thus, ACBUS can be suitable imaging system for therapeutic control or surgical navigation.

All the above-mentioned benefits make ACBUS suitable for use in various clinical applications. The easy and standard scanning protocol makes ACBUS a suitable tool for second-look US instead of handheld ultrasound. With the possibility of image fusion, the location of lesions detected with breast MRI in the ultrasound coordinate system is known which might allow improved lesion classification through the combined used of US and MRI lesion characteristics. Consequently, ACBUS might overcome the increase in false-positive findings and be of value for screening. Next, ACBUS is operator independent and breast volumetric ultrasound images, acquired at different time points can be registered to each other. Thus, ACBUS is a suitable modality for patient follow up. Furthermore, it provides an overview of breast anatomy as depicted by US, which can be used as input for a handheld ultrasound to assist in biopsy planning.

V. Conclusion

The presented study demonstrates a novel US scanning system, called Automated Cone-based Ultrasound Scanner (ACBUS). The system can deliver volumetric breast images whit an image quality similar to the images delivered by a currently commercially available volumetric breast scanner, the Siemens ABVS.

It was demonstrated that ACBUS image data can be fused with MRI image data with a relatively small error. The anatomical correspondence between breast lesions on ACBUS and MRI was confirmed in vivo, and makes ACBUS a suitable independent or second-look imaging modality.

Furthermore, ACBUS provides an easy operator-independent protocol that can be standardized. Combined with the abovementioned benefits, it can be concluded that ACBUS is a good candidate to be used in various clinical applications such as second-look US examination, patient follow-up, screening, and biopsy planning. Besides, it has a potential to be used for biopsy guidance and therapy control.

Acknowledgments

The authors want to gratefully acknowledge Mariolina Bruno and Anna Greco for assisting in the in vivo measurements and for their contribution to the ACBUS design for improving patient comfort.

References

[1] J. Ferlay *et al.*, "Cancer incidence and mortality patterns in Europe: Estimates for 40 countries and 25 major cancers in 2018," *Eur J Cancer,* vol. 103, pp. 356-387, Nov 2018.

[2] C. E. DeSantis *et al.*, "Breast cancer statistics, 2019," *CA Cancer J Clin,* vol. 69, no. 6, pp. 438-451, Nov 2019.

[3] J. Peppercorn, "Breast cancer in women under 40," *Oncology (Williston Park),* vol. 23, no. 6, pp. 465-74, May 2009.

[4] J. E. Vogel, C. Chu, M. McCullough, E. Anderson, A. Losken, and G. W. Carlson, "Breast cancer in women under age 40 years: treatment by total mastectomy and reconstruction," *Ann Plast Surg,* vol. 66, no. 5, pp. 557-60, May 2011.

[5] C. A. Gabriel and S. M. Domchek, "Breast cancer in young women," *Breast Cancer Res,* vol. 12, no. 5, p. 212, 2010.

[6] V. van Breest Smallenburg *et al.*, "Trends in breast biopsies for abnormalities detected at screening mammography: a population-based study in the Netherlands," *British Journal of Cancer,* vol. 109, no. 1, pp. 242-248, 2013/07/01 2013.

[7] H. Madjar, "Role of Breast Ultrasound for the Detection and Differentiation of Breast Lesions," *Breast Care (Basel),* vol. 5, no. 2, pp. 109-114, 2010.

[8] I. C. Bennett and M. A. Biggar, "The role of ultrasound in the management of breast disease," *Australas J Ultrasound Med,* vol. 14, no. 2, pp. 25-28, May 2011.

[9] C. Spick and P. A. Baltzer, "Diagnostic utility of second-look US for breast lesions identified at MR imaging: systematic review and meta-analysis," *Radiology,* vol. 273, no. 2, pp. 401-9, Nov 2014.

[10] R. Candelaria and B. D. Fornage, "Second-look US examination of MR-detected breast lesions," (in eng), no. 1097-0096 (Electronic).

[11] R. Girometti, M. Zanotel, V. Londero, M. Bazzocchi, and C. Zuiani, "Comparison between automated breast volume scanner (ABVS) versus hand-held ultrasound as a second look procedure after magnetic resonance imaging," (in eng), no. 1432-1084 (Electronic).

[12] A. Y. Park *et al.*, "Clinical Value of Real-Time Ultrasonography-MRI Fusion Imaging for Second-Look Examination in Preoperative Breast Cancer Patients: Additional Lesion Detection and Treatment Planning," (in eng), no. 1938-0666 (Electronic).

[13] S. Nakano *et al.*, "Fusion of MRI and sonography image for breast cancer evaluation using real-time virtual sonography with magnetic navigation: first experience," *Jpn J Clin Oncol,* vol. 39, no. 9, pp. 552-9, Sep 2009.

[14] H. J. Moon, M. J. Kim, J. H. Yoon, and E.-K. Kim, "Follow-up interval for probably benign breast lesions on screening ultrasound in women at average risk for breast cancer with dense breasts," *Acta Radiologica,* vol. 59, no. 9, pp. 1045-1050, 2018/09/01 2017.

[15] A. Farrokh, H. Erdonmez, F. Schafer, and N. Maass, "SOFIA: A Novel Automated Breast Ultrasound System Used on Patients in the Prone Position: A Pilot Study on Lesion Detection in Comparison

to Handheld Grayscale Ultrasound," *Geburtshilfe Frauenheilkd,* vol. 78, no. 5, pp. 499-505, May 2018.

[16] S. Wojcinski *et al.*, "The Automated Breast Volume Scanner (ABVS): initial experiences in lesion detection compared with conventional handheld B-mode ultrasound: a pilot study of 50 cases," *Int J Womens Health,* vol. 3, pp. 337-46, 2011.

[17] C. Weismann, C. Mayr, H. Egger, and A. Auer, "Breast Sonography - 2D, 3D, 4D Ultrasound or Elastography?," (in eng), *Breast care (Basel, Switzerland),* vol. 6, no. 2, pp. 98-103, 2011.

[18] A. Mundinger, "3D Supine Automated Ultrasound (SAUS, ABUS, ABVS) for Supplemental Screening Women with Dense Breasts," *J Breast Health,* vol. 12, no. 2, pp. 52-55, Apr 2016.

[19] A. Farrokh, N. Maass, L. Treu, T. Heilmann, and F. K. Schafer, "Accuracy of tumor size measurement: comparison of B-mode ultrasound, strain elastography, and 2D and 3D shear wave elastography with histopathological lesion size," *Acta Radiol,* vol. 60, no. 4, pp. 451-458, Apr 2019.

[20] J. A. Shipley *et al.*, "Automated quantitative volumetric breast ultrasound data-acquisition system," (in eng), no. 0301-5629 (Print).

[21] T. Hopp, P. Baltzer, M. Dietzel, W. A. Kaiser, and N. V. Ruiter, "2D/3D image fusion of X-ray mammograms with breast MRI: visualizing dynamic contrast enhancement in mammograms," *Int J Comput Assist Radiol Surg,* vol. 7, no. 3, pp. 339-48, May 2012.

[22] M. Danch-Wierzchowska, D. Borys, and A. Swierniak, "FEM-based MRI deformation algorithm for breast deformation analysis," *Biocybernetics and Biomedical Engineering,* 2020/08/23/ 2020.

[23] J. S. Schreiman, J. J. Gisvold, J. F. Greenleaf, and R. C. Bahn, "Ultrasound transmission computed tomography of the breast," *Radiology,* vol. 150, no. 2, pp. 523-530, 1984/02/01 1984.

[24] B. Ranger *et al.*, "Breast ultrasound tomography versus MRI for clinical display of anatomy and tumor rendering: preliminary results," (in eng), *AJR. American journal of roentgenology,* vol. 198, no. 1, pp. 233-239, 2012.

[25] N. V. Ruiter, M. Zapf, R. Dapp, T. Hopp, and H. Gemmeke, "First in vivo results with 3D ultrasound computer tomography," in *2012 IEEE International Ultrasonics Symposium*, 2012, pp. 1-4.

[26] C. Liu, C. Xue, B. Zhang, G. Zhang, and C. He, "The Application of an Ultrasound Tomography Algorithm in a Novel Ring 3D Ultrasound Imaging System," (in eng), *Sensors (Basel, Switzerland),* vol. 18, no. 5, p. 1332, 2018.

[27] J. Wiskin, S. A. Borup Dt Fau - Johnson, M. Johnson Sa Fau - Berggren, and M. Berggren, "Non-linear inverse scattering: high resolution quantitative breast tissue tomography," (in eng), no. 1520-8524 (Electronic).

[28] N. Duric and P. Littrup, "Breast Ultrasound Tomography," 2017.

[29] M. W. Lenox, J. Wiskin, M. A. Lewis, S. Darrouzet, D. Borup, and S. Hsieh, "Imaging Performance of Quantitative Transmission Ultrasound," *International Journal of Biomedical Imaging,* vol. 2015, p. 454028, 2015/10/28 2015.

[30] R. M. Mann *et al.*, "Breast MRI: EUSOBI recommendations for women's information," *Eur Radiol,* vol. 25, no. 12, pp. 3669-78, Dec 2015.

[31] G. Weijers, J. M. Thijssen, and C. L. de Korte. (2020, April). *Quality Assurance 4 medical UltraSound equipment*. Available: http://music.radboudimaging.nl/index.php/MUSIC_qa4us

[32] J. M. Thijssen, G. Weijers, and C. L. de Korte, "Objective performance testing and quality assurance of medical ultrasound equipment," *Ultrasound Med Biol,* vol. 33, no. 3, pp. 460-71, Mar 2007.

[33] C. Kollmann *et al.*, "Guideline for Technical Quality Assurance (TQA) of ultrasound devices (B-Mode)--version 1.0 (July 2012): EFSUMB Technical Quality Assurance Group--US-TQA/B," *Ultraschall Med,* vol. 33, no. 6, pp. 544-9, Dec 2012.

[34] J. Ma, "Dixon techniques for water and fat imaging," *J Magn Reson Imaging,* vol. 28, no. 3, pp. 543-58, Sep 2008.

[35] M. H. Mozaffari and W. S. Lee, "Freehand 3-D Ultrasound Imaging: A Systematic Review," *Ultrasound Med Biol,* vol. 43, no. 10, pp. 2099-2124, Oct 2017.

[36] O. V. Solberg, F. Lindseth, H. Torp, R. E. Blake, and T. A. Nagelhus Hernes, "Freehand 3D ultrasound reconstruction algorithms--a review," *Ultrasound Med Biol,* vol. 33, no. 7, pp. 991-1009, Jul 2007.

[37] R. Rohling, A. Gee, and L. Berman, "A comparison of freehand three-dimensional ultrasound reconstruction techniques," *Med Image Anal,* vol. 3, no. 4, pp. 339-59, Dec 1999.

[38] P. J. Besl and N. D. McKay, "A method for registration of 3-D shapes," *IEEE Transactions on Pattern Analysis and Machine Intelligence,* vol. 14, no. 2, pp. 239-256, 1992.

[39] A. Fedorov *et al.*, "3D Slicer as an image computing platform for the Quantitative Imaging Network," *Magn Reson Imaging,* vol. 30, no. 9, pp. 1323-41, Nov 2012.

[40] M. C. van Wijk and J. M. Thijssen, "Performance testing of medical ultrasound equipment: fundamental vs. harmonic mode," *Ultrasonics,* vol. 40, no. 1-8, pp. 585-91, May 2002.

[41] N. J. van Hees *et al.*, "Quantitative ultrasound imaging of healthy and reconstructed cleft lip: a feasibility study," *Cleft Palate Craniofac J,* vol. 44, no. 3, pp. 261-8, May 2007.

[42] Z. Zhou *et al.*, "Classification of Benign and Malignant Breast Tumors in Ultrasound Images with Posterior Acoustic Shadowing Using Half-Contour Features," *Journal of Medical and Biological Engineering,* vol. 35, no. 2, pp. 178-187, 2015/04/01 2015.

[43] S. P. Weinstein, E. F. Conant, C. Mies, G. Acs, S. Lee, and C. Sehgal, "Posterior acoustic shadowing in benign breast lesions: sonographic-pathologic correlation," *J Ultrasound Med,* vol. 23, no. 1, pp. 73-83, Jan 2004.

[44] B. Holländer, G. A. G. M. Hendriks, R. M. Mann, H. H. G. Hansen, and C. L. de Korte, "Plane-Wave Compounding in Automated Breast Volume Scanning: A Phantom-Based Study," *Ultrasound in Medicine & Biology,* vol. 42, no. 10, pp. 2493-2503, 2016/10/01/ 2016.